COLOR IMAGE DENOISING USING QUATERNION ADAPTIVE NON-LOCAL COUPLED MEANS

Xiaoyao Li[1,2]*, Yicong Zhou*[2]*, Jing Zhang*[1]

[1]College of Electrical and Information Engineering, Hunan University, Changsha 410082, China
[2]Department of Computer and Information Science, University of Macau, Macau 999078, China
lxyimayday@gmail.com, yicongzhou@um.edu.mo, zhangj@hnu.edu.cn

ABSTRACT

Because quaternion representation is able to preserve the relationship among RGB channels of a color image, we take advantage of this characteristic and propose a new color image denoising method, named the Quaternion Adaptive Non-local Coupled Means (QANLCM). QANLCM first builds a four-variable optimization model by decomposing the original noisy image into a luminance component and a chromaticity component, and then alternatively updates the four variables in each denoising iteration. Simulations and comparisons demonstrate that QANLCM shows a superiority to other non-local means methods in removing Gaussian noise from color images.

***Index Terms*—** Color image denoising, non-local means, quaternion adaptive non-local coupled means

1. INTRODUCTION

During image acquisition, transmission and storage, images are often contaminated by noise. This will degrade the quality of images and seriously affects the subsequent image processing. Since image denoising aims at removing noise and keeping the details, it plays an important role in image processing.

In 2005, Buades proposed non-local means (NLM) [1–3] for image denoising. Unlike local and pixel-based denoising methods, such as Wiener filter [4] and bilateral filter [5, 6], which utilize a pixel as a unit and usually operate in a local neighbourhood, NLM takes an image patch as a processing unit and aims at obtaining the target image patch by calculating the weighted average of all the image patches in a given search window.

Based on the framework of NLM, people advanced various improvement methods, for example, non-local Euclidean medians (NLEM) [7], improved NLEM (INLEM) [8], non-local patch regression (NLPR) [9], probabilistic NLM (PNLM) [10] and NLM with local James-Stein type center pixel weights (LJS-NLM) [11]. These NLM-based denoising methods calculate the weight ω_{ij} only once and make it unchanged in the later denoising processes. This is inappropriate because the similarity between two image pixels/patches will change after each denoising iteration. Considering this issue, Lan and Zhou [12] proposed non-local fuzzy means (NLFM) which takes the weight ω_{ij} as an optimization variable and iteratively updates its value. By inheriting this advantage of NLFM and replacing the Euclidean distance with unbiased distance, unbiased distance based non-local fuzzy means (UDNLFM) [13] was proposed recently. However, most of these existing NLM-based denoising methods yield poor results in color image denoising, because they treat each color channel as an independent component and ignore the relationships among different color channels.

In this paper, we will propose a new color image denoising method, named the Quaternion Adaptive Non-local Coupled Means (QANLCM). Unlike many existing NLM-based denoising methods, QANLCM can process all the color channels as a whole in RGB space. In QANLCM, we first utilize quaternion unit transform to decompose the original image into a luminance component and a chromaticity component, and then build an optimization model with four variables. QANLCM is more proper than the one only using color intensity information in optimization model. Similar to NLFM, the proposed method treats weight ω_{ij} and υ_{ij} as optimization variables and updates their values in each iteration. Related experiments are implemented to show the excellent denoising capability of our method.

2. BACKGROUND

2.1. Quaternion representation of color image

A quaternion number q is a hypercomplex number, which consists of one real part and three imaginary parts [14]

$$q = A + B\mathbf{i} + C\mathbf{j} + D\mathbf{k}, \tag{1}$$

This work was supported in part by the Macau Science and Technology Development Fund under Grant FDCT/189/2017/A3, and by the Research Committee at University of Macau under Grants MYRG2016-00123-FST and MYRG2018-00136-FST.

where A, B, C and D are real numbers, and **i**, **j**, **k** are complex operators satisfying the following rules

$$\begin{cases} \mathbf{i}^2 = \mathbf{j}^2 = \mathbf{k}^2 = \mathbf{ijk} = -1, \\ \mathbf{ij} = \mathbf{k}, \mathbf{jk} = \mathbf{i}, \mathbf{ki} = \mathbf{j}, \\ \mathbf{ji} = -\mathbf{k}, \mathbf{kj} = -\mathbf{i}, \mathbf{ik} = -\mathbf{j}. \end{cases} \tag{2}$$

As can be seen, q is a pure quaternion when $A = 0$. In addition, the conjugate and the modulus of quaternion q are defined as

$$\bar{q} = A - B\mathbf{i} - C\mathbf{j} - D\mathbf{k}, \tag{3}$$

$$|q| = \sqrt{q\bar{q}} = \sqrt{\bar{q}q} = \sqrt{A^2 + B^2 + C^2 + D^2}. \tag{4}$$

In the RGB domain, a color image consists of three color channels, i.e. the red, green and blue channels. We can use a pure quaternion to represent a color pixel as $q = r\mathbf{i} + g\mathbf{j} + b\mathbf{k}$, where r,g,b represent the pixel values in the red, green, blue channels, respectively. Thus, a three-dimensional color pixel can be processed as a whole.

If given $\mu = (\mathbf{i} + \mathbf{j} + \mathbf{k})/\sqrt{3}$, the related unit quaternion U can be represented as $T = |T|e^{\mu\theta} = \cos\theta + \mu\sin\theta$. Then we can define the quaternion unit transform of a color pixel q as follows [15]

$$\begin{aligned} TqT &= [\cos\theta + \mu\sin\theta](r\mathbf{i} + g\mathbf{j} + b\mathbf{k})[\cos\theta - \mu\sin\theta] \\ &= q^{RGB} + q^L + q^\Delta, \end{aligned} \tag{5}$$

and

$$\bar{T}qT = q^{RGB} + q^L - q^\Delta, \tag{6}$$

where

$$\begin{cases} q^{RGB} &= (r\mathbf{i} + g\mathbf{j} + b\mathbf{k})\cos 2\theta, \\ q^L &= \frac{2}{\sqrt{3}}\mu(r + g + b)\sin^2\theta, \\ q^\Delta &= \frac{1}{\sqrt{3}}[(b - g)\mathbf{i} + (r - b)\mathbf{j} + (g - r)\mathbf{k}]\sin 2\theta. \end{cases} \tag{7}$$

q^L and q^Δ denote the luminance and chromaticity component [16] of the color pixel q, respectively.

2.2. NLM

Supposed noisy image $\mathbf{Y} = \mathbf{X} + \mathbf{N}$, where $\mathbf{X}$ denotes the corresponding clean image and $\mathbf{N}$ denotes Gaussian noise, NLM obtains the denoised image $\hat{\mathbf{X}}$ by

$$\hat{\mathbf{X}}_i = \sum_{j \in \mathbf{S}_i} \omega_{ij} \mathbf{Y}_j, \tag{8}$$

where

$$\omega_{ij} = \frac{1}{W} \cdot \exp\left(-\frac{||\mathbf{Y}_i - \mathbf{Y}_j||^2}{h^2}\right), \tag{9}$$

$$W = \sum_{j \in \mathbf{S}_i} \exp\left(-\frac{||\mathbf{Y}_i - \mathbf{Y}_j||^2}{h^2}\right). \tag{10}$$

$\hat{\mathbf{X}}_i$ is the denoised image patch centered at pixel i. $\mathbf{Y}_i$ and $\mathbf{Y}_j$ are the noisy image patches centered at pixels i and j. ω_{ij} denotes the weight between patches $\mathbf{Y}_i$ and $\mathbf{Y}_j$. $\mathbf{S}_i$ is the search window with center pixel i and radius s. In addition, the center pixel i is not included in $\mathbf{S}_i$. W is the normalization factor that makes $\sum_{j \in \mathbf{S}_i} \omega_{ij} = 1$. h denotes the smoothing parameter.

3. QANLCM

This section will first review NLFM, then introduce our new denoising method, namely Quaternion Adaptive Non-local Coupled Means (QANLCM), and finally analyze the similarities and differences between NLFM and QANLCM.

3.1. NLFM

Due to the fact that many NLM-based methods compute weight ω_{ij} once and then keep it fixed in the subsequent denoising iterations, NLFM was proposed to treat the weight ω_{ij} as an optimization variable and update its value iteratively. The optimization model of NLFM [12] is given as

$$\{\hat{\mathbf{X}}_i, \omega_{ij}\} = \underset{\mathbf{X}_i, \omega_{ij}}{\arg\min} \sum_{j \in \mathbf{S}_i} \omega_{ij} ||\mathbf{X}_i - \mathbf{Y}_j||^2 + h \sum_{j \in \mathbf{S}_i} \omega_{ij} \log \omega_{ij} \tag{11}$$

where $\omega_{ij} \geq 0$ and $\sum_{j \in \mathbf{S}_i} \omega_{ij} = 1$. We first have the initial settings of $\hat{\mathbf{X}}^{(0)} = \mathbf{Y}$ and $t = 0$, and then alternately update ω_{ij} and $\hat{\mathbf{X}}_i$ by the following equations

$$\omega_{ij}^{(t+1)} = \frac{1}{W} \cdot \exp\left(-\frac{||\hat{\mathbf{X}}_i^{(t)} - \mathbf{Y}_j||^2}{h}\right), \tag{12}$$

$$\hat{\mathbf{X}}_i^{(t+1)} = \sum_{j \in \mathbf{S}_i} \omega_{ij}^{(t+1)} \mathbf{Y}_j. \tag{13}$$

where $t = 0, 1, 2, \cdots$. After $(t+1)$ iterations, we will obtain weight ω_{ij} and the denoised image patch $\hat{\mathbf{X}}_i$ as $\omega_{ij}^{(t+1)}$ and $\hat{\mathbf{X}}_i^{(t+1)}$, respectively. W denotes the normalization factor.

3.2. QANLCM

In this subsection, we propose the Quaternion Adaptive Non-local Coupled Means (QANLCM). Its optimization model is defined as

$$\begin{aligned} &\{\hat{\mathbf{X}}_i^L, \hat{\mathbf{X}}_i^\Delta, \omega_{ij}, \upsilon_{ij}\} = \\ &\underset{\mathbf{X}_i^L, \mathbf{X}_i^\Delta, \omega_{ij}, \upsilon_{ij}}{\arg\min} \quad \|\mathbf{X}_i^L + \mathbf{X}_i^\Delta - \mathbf{Y}_i^L - \mathbf{Y}_i^\Delta\|^2 \\ &\qquad + t \cdot \Big(\sum_{j \in \mathbf{S}_i} \omega_{ij} \|\mathbf{X}_i^L - \mathbf{Y}_j^L\|^2 + h_L \sum_{j \in \mathbf{S}_i} \omega_{ij} \log \omega_{ij} \Big) \\ &\qquad + (1-t) \cdot \Big(\sum_{j \in \mathbf{S}_i} \upsilon_{ij} \|\mathbf{X}_i^\Delta - \mathbf{Y}_j^\Delta\|^2 + h_\Delta \sum_{j \in \mathbf{S}_i} \upsilon_{ij} \log \upsilon_{ij} \Big), \end{aligned} \tag{14}$$

where $\omega_{ij}, \upsilon_{ij} \geq 0$, $\sum_{j \in \mathbf{S}_i} \omega_{ij} = 1$ and $\sum_{j \in \mathbf{S}_i} \upsilon_{ij} = 1$. $\hat{\mathbf{X}}_i^L$, $\mathbf{X}_i^L$, $\mathbf{Y}_i^L$,$\mathbf{Y}_j^L$ are the luminance components and $\hat{\mathbf{X}}_i^\Delta$,$\mathbf{X}_i^\Delta$,$\mathbf{Y}_i^\Delta$,

$\mathbf{Y}_j^{\Delta}$ are the chromaticity components of image patches $\hat{\mathbf{X}}_i$, $\mathbf{X}_i$,$\mathbf{Y}_i$,$\mathbf{Y}_j$, respectively. $t \in (0,1)$ is a trade-off parameter. Based on Eqs. (5)-(7), we let $\theta = \pi/4$ and then obtain $\hat{\mathbf{X}}_i^L$, $\hat{\mathbf{X}}_i^{\Delta}$ as

$$\hat{\mathbf{X}}_i^L = \frac{1}{2}(T\hat{\mathbf{X}}_i\bar{T} + \bar{T}\hat{\mathbf{X}}_i T), \hat{\mathbf{X}}_i^{\Delta} = \frac{1}{2}(T\hat{\mathbf{X}}_i\bar{T} - \bar{T}\hat{\mathbf{X}}_i T). \quad (15)$$

In the same way, we can calculate $\mathbf{Y}_i^L$,$\mathbf{Y}_j^L$, $\mathbf{Y}_i^{\Delta}$ and $\mathbf{Y}_j^{\Delta}$.

To solve the optimization problem of Eq. (14), we initialize $\hat{\mathbf{X}}_i^{(0)} = \mathbf{Y}_i$ and then update $\hat{\mathbf{X}}_i^L$, $\hat{\mathbf{X}}_i^{\Delta}$, ω_{ij} and υ_{ij} as

$$\omega_{ij}^{(t+1)} = \frac{1}{W_L} \cdot \exp\left(-\frac{\|\hat{\mathbf{X}}_i^{L^{(t)}} - \mathbf{Y}_j^L\|^2}{h_L}\right) \cdot H_{ij}, \quad (16)$$

$$\upsilon_{ij}^{(t+1)} = \frac{1}{W_{\Delta}} \cdot \exp\left(-\frac{\|\hat{\mathbf{X}}_i^{\Delta^{(t)}} - \mathbf{Y}_j^{\Delta}\|^2}{h_{\Delta}}\right) \cdot H_{ij}, \quad (17)$$

$$\hat{\mathbf{X}}_i^{L^{(t+1)}} = \frac{\mathbf{Y}_i^L + \mathbf{Y}_i^{\Delta} - \hat{\mathbf{X}}_i^{\Delta^{(t)}} + t \cdot \sum_{j \in \mathbf{S}_i} \omega_{ij}^{(t+1)} \mathbf{Y}_j^L}{1+t}, \quad (18)$$

$$\hat{\mathbf{X}}_i^{\Delta^{(t+1)}} = \frac{\mathbf{Y}_i^L + \mathbf{Y}_i^{\Delta} - \hat{\mathbf{X}}_i^{L^{(t+1)}} + (1-t) \cdot \sum_{j \in \mathbf{S}_i} \upsilon_{ij}^{(t+1)} \mathbf{Y}_j^{\Delta}}{2-t}, \quad (19)$$

where W_L, W_{Δ} are normalization factors and h_L, h_{Δ} are smoothing parameters. The spatial kernel $H_{ij} = \exp\left(-\frac{(i-j)^2}{h_s}\right)$ and h_s denotes the spatial parameter. When the termination is satisfied, the denoising iteration will stop and we can obtain the final denoised result as $\hat{\mathbf{X}}_i = \bar{T}(\hat{\mathbf{X}}_i^L + \hat{\mathbf{X}}_i^{\Delta})T$.

3.3. Comparison of QANLCM and NLFM

By comparing the optimization models and algorithm processes of NLFM and QANLCM, their similarities lie in that they are both NLM-based methods, and take weight ω_{ij} as an optimization variable and iteratively change its value in each denoising iteration. However, the differences between NLFM and QANLCM are listed as follows:

1. NLFM was originally proposed for grayscale image. When being applied to color image, NLFM treats the three color channels as three independent parts. However, QANLCM adopts quaternion representation to keep the relationships among the three color channels.
2. NLFM utilizes the intensity difference to measure the similarity between two image patches, while QANLCM considers both the luminance and chromaticity aspects, and then it is more appropriate to deal with a color image.
3. NLFM has two optimization variables ($\hat{\mathbf{X}}_i$ and ω_{ij}), while QANLCM has four variables ($\hat{\mathbf{X}}_i^L$, $\hat{\mathbf{X}}_i^{\Delta}$, ω_{ij} and υ_{ij}) to be optimized.

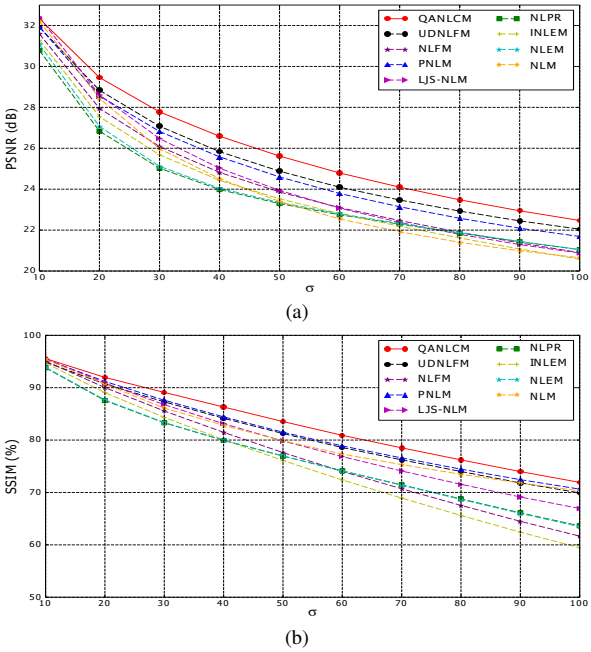

Fig. 1. Average values of (a) PSNR and (b) SSIM on the test images.

4. EXPERIMENTS

In this section, we compare our QANLCM with several existing NLM-based methods. They are traditional NLM [1], NLEM [7], INLEM [8], NLPR [9], LJS-NLM [11], PNLM [10], NLFM [12] and UDNLFM [13]. These competing denoising methods are applied to denoise each color channel independently in RGB space, and then merge three denoised channels to acquire the denoised color image. The experiments are conducted on forty test color images.

Fig. 1 displays the average PSNR and structural similarity (SSIM) [17] values on all the test images. In Fig. 1(a), QANLCM and UDNLFM stay above 22dB when noise level $\sigma = 100$. However, in the same situation, other competing methods except PNLM fall below 21dB. When $\sigma > 20$, QANLCM surpasses UDNLFM, PNLM and NLFM by about 0.8dB, 1.0dB and 1.8dB, respectively. According to average SSIM shown in Fig. 1(b), QANLCM achieves more than 70% even when noise level $\sigma = 100$. However, NLEM, INLEM, NLPR and NLFM drop below 70% when $\sigma \geq 70$. QANLCM, UDNLFM and PNLM outperform NLFM in all situations. QANLCM exceeds PNLM and UDNLFM by about 3% when $\sigma > 20$. Table 1 shows the results on three test images with noise level σ ranging from 10 to 100. As can be seen, QANLCM outperforms other competing denoising methods in terms of PSNR and SSIM.

Fig. 2 displays the denoised results of the *lena* image with noise level $\sigma = 20$. Compared with the clean image in Fig. 2(a), we notice that NLEM, INLEM and NLPR cause blur in their denoised images, especially in the area of the purple

Table 1. PSNR and SSIM results of QANLCM and other methods at noise levels $\sigma = 10, 20, \cdots, 100$.

Image	Method\σ	PSNR(dB) 10	20	30	40	50	60	70	80	90	100	SSIM(%) 10	20	30	40	50	60	70	80	90	100
airplane	**QANLCM**	**33.36**	**29.63**	**27.91**	**26.53**	**25.60**	**24.64**	**23.81**	**23.25**	**22.59**	**22.05**	**94.58**	**90.12**	**87.10**	**83.36**	**78.90**	**75.15**	**70.59**	**67.18**	**63.64**	**60.17**
	UDNLFM [13]	32.28	28.57	26.66	25.25	24.16	23.24	22.50	21.98	21.51	21.06	92.89	88.29	84.17	79.85	74.64	70.56	66.36	62.48	58.87	55.76
	NLFM [12]	31.57	27.39	25.44	24.00	22.98	22.21	21.64	21.17	20.69	20.27	92.48	85.83	78.86	71.54	64.11	58.71	53.46	49.20	44.99	42.06
	PNLM [10]	31.75	27.84	26.14	24.90	23.84	22.94	22.23	21.69	21.18	20.69	92.77	88.19	84.26	80.11	75.41	71.49	67.74	64.29	61.11	57.40
	LJS-NLM [11]	32.21	28.20	26.01	24.41	23.27	22.30	21.56	20.97	20.48	20.03	92.71	87.46	82.11	76.59	71.03	66.43	61.55	57.72	54.00	50.32
	NLPR [9]	30.93	26.23	23.87	22.69	22.10	21.63	21.28	21.00	20.60	20.30	91.39	83.74	75.87	69.36	63.37	59.16	54.77	51.04	46.86	44.38
	INLEM [8]	31.35	27.00	24.91	23.45	22.58	21.91	21.40	20.96	20.47	20.04	92.03	84.42	76.33	68.29	60.87	55.62	50.53	46.49	42.38	39.56
	NLEM [7]	31.22	26.59	23.99	22.78	22.17	21.69	21.33	21.02	20.63	20.31	91.71	84.05	75.96	69.51	63.43	59.11	54.66	50.83	46.75	44.11
	NLM [1]	32.22	28.57	25.72	24.21	23.08	21.88	21.19	20.60	20.18	19.77	93.22	88.14	83.05	78.53	73.85	70.86	66.90	63.84	61.60	58.54
	Noisy Image	28.15	22.11	18.60	16.09	14.14	12.57	11.23	10.08	9.05	8.16	71.55	50.04	38.22	30.20	24.41	20.05	16.69	14.05	11.92	10.19
headlight	**QANLCM**	**32.05**	**28.25**	**26.40**	**25.07**	**24.20**	**23.38**	**22.65**	**22.24**	**21.78**	**21.43**	**96.27**	**91.57**	**87.89**	**84.20**	**80.79**	**77.54**	**74.24**	**72.08**	**69.67**	**67.19**
	UDNLFM [13]	30.96	26.95	24.97	23.65	22.81	22.16	21.61	21.23	20.89	20.57	94.79	89.29	84.34	80.01	76.54	73.45	70.56	68.68	66.55	64.48
	NLFM [12]	30.64	26.34	24.31	23.03	22.20	21.63	21.11	20.72	20.33	19.95	95.01	88.84	82.57	77.64	73.63	69.90	66.29	63.78	60.56	57.65
	PNLM [10]	30.71	26.37	24.72	23.54	22.66	22.01	21.42	21.02	20.61	20.32	95.16	89.61	84.67	80.28	76.64	73.43	70.83	68.77	66.78	64.68
	LJS-NLM [11]	31.27	26.98	24.76	23.33	22.37	21.65	21.03	20.60	20.19	19.87	95.38	89.65	84.28	79.81	76.11	72.65	69.51	67.24	64.77	62.36
	NLPR [9]	30.16	24.69	22.76	21.92	21.46	21.16	20.83	20.57	20.28	20.00	94.00	83.94	77.58	74.44	71.71	69.17	66.41	64.54	61.87	59.48
	INLEM [8]	30.53	25.93	23.78	22.62	21.92	21.42	20.94	20.55	20.14	19.75	94.76	87.37	80.66	76.08	72.24	68.54	64.77	62.11	58.64	55.56
	NLEM [7]	30.31	24.73	22.80	22.00	21.54	21.23	20.88	20.61	20.32	20.02	94.06	83.66	77.62	74.58	71.88	69.25	66.48	64.52	61.84	59.36
	NLM [1]	31.19	26.98	24.18	22.92	22.03	21.17	20.64	20.26	19.94	19.70	95.12	89.50	82.67	78.84	75.63	71.64	69.48	67.81	66.31	64.79
	Noisy Image	28.12	22.12	18.59	16.08	14.16	12.57	11.21	10.08	9.04	8.12	87.50	67.98	51.97	40.39	31.90	25.52	20.61	17.31	14.43	12.28
lena	**QANLCM**	**33.14**	**29.92**	**28.36**	**27.22**	**26.35**	**25.43**	**24.60**	**23.95**	**23.50**	**22.91**	**99.04**	**98.11**	**97.54**	**96.62**	**95.80**	**94.81**	**93.87**	**92.93**	**92.04**	**91.13**
	UDNLFM [13]	32.65	29.35	27.53	26.15	25.17	24.32	23.61	23.07	22.55	22.18	98.86	97.71	96.56	95.34	94.38	93.35	92.36	91.61	90.67	89.97
	NLFM [12]	31.80	28.23	26.35	25.02	24.11	23.31	22.63	22.09	21.55	21.06	98.68	97.24	95.81	94.47	93.31	92.15	90.98	89.82	88.44	87.25
	PNLM [10]	32.18	28.83	27.20	25.81	24.82	23.84	23.02	22.40	21.90	21.45	98.75	97.52	96.44	95.24	94.19	93.09	92.05	91.16	90.33	89.56
	LJS-NLM [11]	32.59	28.79	26.60	24.99	23.83	22.83	22.03	21.42	20.94	20.43	98.87	97.49	96.10	94.71	93.49	92.24	91.21	90.14	89.19	88.18
	NLPR [9]	31.06	27.01	25.19	24.22	23.62	23.02	22.48	22.08	21.63	21.24	98.40	96.29	94.66	93.64	92.84	91.96	91.02	90.15	89.01	88.11
	INLEM [8]	31.45	27.86	25.91	24.67	23.84	23.08	22.41	21.86	21.29	20.77	98.56	96.95	95.37	94.06	92.92	91.71	90.46	89.16	87.59	86.22
	NLEM [7]	31.48	27.21	25.27	24.27	23.67	23.07	22.52	22.10	21.64	21.23	98.53	96.36	94.70	93.67	92.86	91.98	91.05	90.14	88.99	88.06
	NLM [1]	31.92	28.38	25.98	24.39	23.19	22.29	21.52	20.95	20.52	20.07	98.73	97.35	95.64	94.31	93.10	91.80	90.89	89.97	89.22	88.47
	Noisy Image	28.15	22.11	18.60	16.09	14.13	12.54	11.26	10.08	9.06	8.12	96.73	88.48	77.96	67.20	57.34	48.81	41.99	35.79	30.93	26.71

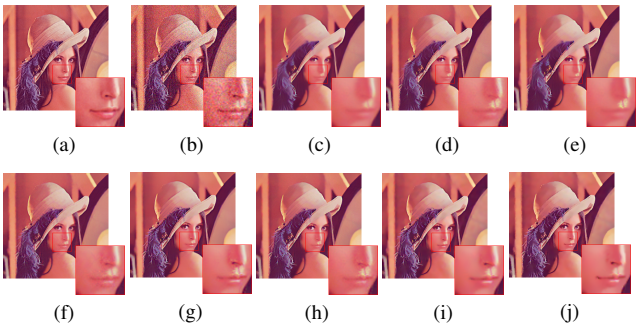

Fig. 2. Denoised results of the *lena* image with noise $\sigma = 20$: (a) clean image; (b) noisy image; (c) NLEM; (d) INLEM; (e) NLPR; (f) LJS-NLM; (g) PNLM; (h) NLFM; (i) UDNLFM; (j) QANLCM.

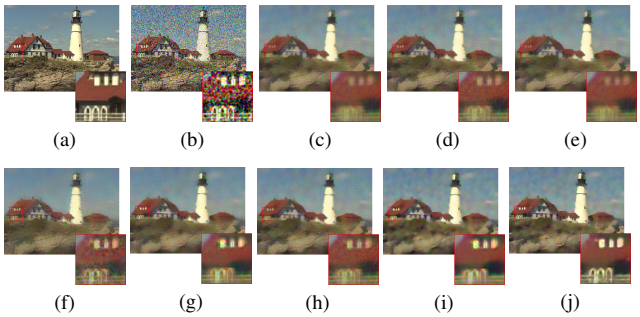

Fig. 3. Denoised results of the *headlight* image with noise $\sigma = 70$: (a) clean image; (b) noisy image; (c) NLEM; (d) INLEM; (e) NLPR; (f) LJS-NLM; (g) PNLM; (h) NLFM; (i) UDNLFM; (j) QANLCM.

feather on the hat. From the zoom-in part of these denoised results, NLEM, INLEM, NLPR, LJS-NLM and NLFM lose some details in the face, such as the corner of the mouth and nostril. And for the result of PNLM in Fig. 2(g), there are still some obvious noises shown on the philtrum. QANLCM and UDNLFM achieve better performance than other methods in maintaining the detail information and in reducing noise. Fig. 3 shows another group of denoised results of the *headlight* image with noise $\sigma = 70$. As can be seen from the zoom-in part, we can distinguish some structure information of the white fence in the results of LJS-NLM, PNLM, UDNLFM and QANLCM, while other methods lose most of the details and result in over-smoothed images. Although LJS-NLM performs well in detail preservation, it introduces many artifacts in the denoised image. Compared with the competing denosing methods, QANLCM retains more details and structure informations, such as the windows of the houses and the texture of rocks.

In summary, both quantitative analysis and visual comparison demonstrate that our QANLCM achieves better denoising performance than other NLM-based denoising methods over a wide range of noise levels.

5. CONCLUSION

Based on quaternion representation of the color image, we proposed a new image denoising method, named the Quaternion Adaptive Non-local Coupled Means (QANLCM). It can denoise three color channels as a whole. Different from those methods which calculate image pixel/patch distance by directly using color intensity, QANLCM splits the original image into a luminance component and a chromaticity component, and then considers both components when measuring color image pixel/patch similarity. Similar to NLFM, QANLCM takes weight ω_{ij} and v_{ij} as optimization variables and changes their values iteratively. Quantitative analysis and visual results showed that QANLCM achieves excellent denoising performance in removing noise and retaining details.

6. REFERENCES

[1] Antoni Buades, Bartomeu Coll, and Jean-Michel Morel, "A non-local algorithm for image denoising," in *2005 IEEE Computer Society Conference on Computer Vision and Pattern Recognition (CVPR'05)*, June 2005, vol. 2, pp. 60–65.

[2] Antoni Buades, Bartomeu Coll, and Jean-Michel Morel, "Non-local means denoising," *Image Processing On Line*, vol. 1, pp. 208–212, 2011.

[3] Antoni Buades, Bartomeu Coll, and Jean-Michel Morel, "A review of image denoising algorithms, with a new one," *SIAM Journal on Multiscale Modeling and Simulation*, vol. 4, no. 2, pp. 490–530, 2005.

[4] Xiaodi Huang and G. A. Woolsey, "Image denoising using wiener filtering and wavelet thresholding," in *2000 IEEE International Conference on Multimedia and Expo.*, 2000, vol. 3, pp. 1759–1762.

[5] Carlo Tomasi and Roberto Manduchi, "Bilateral filtering for gray and color images," in *6th International Conference on Computer Vision*, 1998, pp. 839–846.

[6] Michael Elad, "On the origin of the bilateral lter and ways to improve it," *IEEE Transactions on Image Processing*, vol. 10, no. 10, pp. 1141–1151, 2002.

[7] Kunal N. Chaudhury and Amit Singer, "Non-local euclidean medians," *IEEE Signal Processing Letters*, vol. 19, no. 11, pp. 745–748, 2012.

[8] Zhonggui Sun and Songcan Chen, "Analysis of non-local euclidean medians and its improvement," *IEEE Signal Processing Letters*, vol. 20, no. 4, pp. 303–306, 2013.

[9] Kunal N. Chaudhury and Amit Singer, "Non-local patch regression: Robust image denoising in patch space," in *2013 IEEE International Conference on Acoustics, Speech and Signal Processing*, 2013, pp. 1345–1349.

[10] Yue Wu, Brain Tracey, Premkumar Natarajan, and Joseph P. Noonan, "Probabilistic non-local means," *IEEE Signal Processing Letters*, vol. 20, no. 8, pp. 763–766, 2013.

[11] Yue Wu, Brain Tracey, Premkumar Natarajan, and Joseph P. Noonan, "James-stein type center pixel weights for non-local means image denoising," *IEEE Signal Processing Letters*, vol. 20, no. 4, pp. 411–414, 2013.

[12] Rushi Lan, Yicong Zhou, Yuan Yan Tang, and C. L. Philip Chen, "Image denoising using non-local fuzzy means," in *2015 IEEE China Summit and International Conference on Signal and Information Processing (ChinaSIP)*, 2015, pp. 196–200.

[13] Xiaoyao Li, Yicong Zhou, Jing Zhang, and Lianhong Wang, "Unbiased distance based non-local fuzzy means," in *2018 IEEE International Conference on Acoustics, Speech and Signal Processing*, 2018, pp. 1423–1427.

[14] William Rowan Hamilton, "Scientific books: Elements of quaternions," vol. 14, pp. 65–66, 1901.

[15] Canhui Cai and S. K. Mitra, "A normalized color difference edge detector based on quaternion representation," in *Proceedings 2000 International Conference on Image Processing*, 2000, vol. 2, pp. 816–819 vol.2.

[16] Konstantinos N. Plataniotis and Anastasios N. Venetsanopoulos, "Color image processing and applications," *Springer-Verlag New York, Inc.*, 2000.

[17] Zhou Wang, Alan Conrad Bovik, Hamid Rahim Sheikh, and Eero P. Simoncelli, "Image quality assessment: from error visibility to structural similarity," *IEEE Transactions on Image Processing*, vol. 13, no. 4, pp. 600–612, 2004.